Astronomy & Astrophysics manuscript no. helix_v11
November 18, 2014

©ESO 2014

arXiv:1411.4429v1 [astro-ph.SR] 17 Nov 2014

Herschel imaging of the dust in the Helix Nebula (NGC 7293)*

G. C. Van de Steene[1,**], P. A. M. van Hoof[1], K. M. Exter[2], M. J. Barlow[3], J. Cernicharo[10], M. Etxaluze[10], W. K. Gear[6], J. R. Goicoechea[10], H. L. Gomez[6], M. A. T. Groenewegen[1], P. C. Hargrave[6], R. J. Ivison[4], S. J. Leeks[7], T. L. Lim[7], M. Matsuura[3], G. Olofsson[8], E. T. Polehampton[7,9], B. M. Swinyard[7], T. Ueta[5], H. Van Winckel[2], C. Waelkens[2], and R. Wesson[3,11]

[1] Royal Observatory of Belgium, Ringlaan 3, B-1180 Brussels, Belgium
[2] Instituut voor Sterrenkunde, Katholieke Universiteit Leuven, Celestijnenlaan 200 D, B-3001 Leuven, Belgium
[3] Dept of Physics & Astronomy, University College London, Gower St, London WC1E 6BT, UK
[4] UK Astronomy Technology Centre, Royal Observatory Edinburgh, Blackford Hill, Edinburgh EH9 3HJ, UK
[5] Dept. of Physics and Astronomy, University of Denver, Mail Stop 6900, Denver, CO 80208, USA
[6] School of Physics and Astronomy, Cardiff University, 5 The Parade, Cardiff, Wales CF24 3YB, UK
[7] Space Science and Technology Department, Rutherford Appleton Laboratory, Oxfordshire, OX11 0QX, UK
[8] Dept. of Astronomy, Stockholm University, AlbaNova University Center, Roslagstullsbacken 21, 10691 Stockholm, Sweden
[9] Department of Physics, University of Lethbridge, Lethbridge, Alberta, T1J 1B1, Canada
[10] Instituto de Ciencia de Materiales (ICMM-CSIC), Calle Sor Juana Ines de la Cruz, 3, Cantoblanco, 28049 Madrid, Spain
[11] European Southern Observatory, Alonso de Cordova 3107, Casilla 19001, Santiago, Chile

Received ; Accepted

ABSTRACT

Aims. In our series of papers presenting the *Herschel* imaging of evolved planetary nebulae, we present images of the dust distribution in the Helix nebula (NGC 7293).
Methods. Images at 70, 160, 250, 350, and 500 μm were obtained with the PACS and SPIRE instruments on board the Herschel satellite.
Results. The broadband maps show the dust distribution over the main Helix nebula to be clumpy and predominantly present in the barrel wall. We determined the spectral energy distribution of the main nebula in a consistent way using Herschel, IRAS, and Planck flux values. The emissivity index of $\beta = 0.99 \pm 0.09$, in combination with the carbon rich molecular chemistry of the nebula, indicates that the dust consists mainly of amorphous carbon. The dust excess emission from the central star disk is detected at 70 μm and the flux measurement agree with previous measurement. We present the temperature and dust column density maps. The total dust mass across the Helix nebula (without its halo) is determined to be 3.5 10^{-3} $M_\odot$ at a distance of 216 pc. The temperature map shows dust temperatures between 22 and 42 K, which is similar to the kinetic temperature of the molecular gas, strengthening the fact that the dust and gas co-exist in high density clumps. Archived images are used to compare the location of the dust emission in the far infrared (*Herschel*) with the ionized (GALEX Hβ) and molecular (H_2) component. The different emission components are consistent with the Helix consisting of a thick walled barrel-like structure inclined to the line of sight. The radiation field decreases rapidly through the barrel wall.

Key words. planetary nebulae: individual: NGC 7293 – circumstellar matter – dust – Infrared: ISM

1. Introduction

We present *Herschel* observations of the Planetary Nebula (PN) NGC 7293, also known as the Helix nebula, which is the nearest, large PN at a distance of 216^{+14}_{-12} pc (**?**), allowing us to study its spatial structure in detail. The white dwarf central star WD 2226-210 with a surface temperature of 103 600 ± 5500 K (**?**) ionizes the AGB nebula. **?** also showed the presence of a 35-150 AU diameter debris disk around this central star.

The Helix has been extensively studied over a wide range of wavelengths with ground- and space-based telescopes. At optical wavelengths, neutral and ionized atomic gas has been well-characterized by the Hubble Space Telescope (HST; **??**). Observations in H_2 have identified the presence of numerous globules in the Helix, often observed with cometary-like tails in H_2, CO, and at infrared wavelengths (**?????**). A map encompassing the region of the optical image in the CO J=2−1 transition has been made by **??**. More complex molecules, including HCN, CN, HCO^+, CCH, C_3H_2, and H_2CO, HCO^+ have also been detected in dense gas in the Helix (**???**). Most recently **?** studied the spatial distribution of the atomic and molecular gas along the western rim in the submillimeter range with the SPIRE instrument on board Herschel.

Understanding the complex morphology of the Helix nebula has been the subject of numerous studies (**???**, e.g.[]). One major obstacle has been a lack of high resolution velocity data, until recently when **?** observed the J = 1−0 transition of HCO^+ at 89 GHz across the Helix nebula with a velocity resolution of 1.68 km/s and an angular resolution of 35″ (half beamwidth). The image constructed from HCO^+ emission closely resembles that observed in the optical, as well as in vibrationally excited H_2, suggesting a common morphology. The high resolution spectra

---

* Herschel is an ESA space observatory with science instruments provided by European-led Principal Investigator consortia and with important participation from NASA.

** gsteene@oma.be

obtained in HCO^+ indicate a barrel-like, bipolar outflow tilted about 10° east relative to the line of sight. Around this main nebula is a 40′ diameter halo which shows interaction with the ISM in the NE (**??**).

The reason for studying NGC 7293 is its similarity to the other highly evolved planetary nebulae which are also part of the MESS program: the Ring nebula (NGC 6720) (**?**) and the Little Dumbbell Nebula (NGC 650) (**?**). Both nebulae have a highly evolved central star and exhibit high density, cometary knots.

In this paper we discuss far infrared images obtained with the PACS and SPIRE instruments on board the *Herschel* telescope in sections 2 and 3. We present the SED in section 4, the temperature map in section 5 and mass column density map in section 6. The properties of the central star disk is discussed in section 7. In section 8 we compare the dust component with images of the molecular and ionized component. The conclusions are presented in section 9.

2. Observations and data reduction

As part of the *Herschel* guarantee time key project MESS (Mass loss of Evolved StarS) (P.I. Martin Groenewegen) we have imaged a sample of planetary nebulae (PNe) with the PACS (**?**) and SPIRE (**?**) instruments on board the *Herschel* satellite (**?**). A detailed description of the program can be found in **?**. An overview of the *Herschel* observations of PNe in the MESS program was presented in **?**. Other PNe have been observed in the *Herschel* Planetary Nebulae Survey (**?**). In this article we will present the *Herschel* PACS and SPIRE observations of the Helix nebula obtained in the framework of the MESS Program and the deep SPIRE photometer maps obtained in the framework of the Must-Do 7 proposal led by J. Cernicharo.

PACS has three wavelength channels, 70 μm (blue channel), 100 μm (green), and 160 μm (red), with two observed simultaneously, red and blue in our case. SPIRE operates at 250 μm (PSW band), 350 μm (PMW), and 500 μm (PLW) simutaneously. We obtained both SPIRE and PACS data simultaneously in parallel mode at 60″/s scan speed. SPIRE observations were also redone as MustDo (MD) observations at a scan speed of 30″/s. The log of the observations is presented in Table 1.

To generate broadband images, we used the *Herschel* Interactive Processing Environment (HIPE, version 10.0; **?**) and the Scanamorphos data reduction tool (Scanamorphos, version 20; **?**). We used the same pixel size for the PACS 70 and 160 μm images being 2.″85, and the standard Scanamorphos pixel sizes of 4.″5, 6.″25, and 9″for the SPIRE images. The FWHM of the PACS beam at 70 and 160 μm is 5.″7 and 11.″4, respectively. The FWHM of the SPIRE beam sizes are 18.″1, 25.″2, and 36.″6, at 250, 350, 500 μm, respectively. The PACS images are in Jy/pixel, while SPIRE images are in Jy/sr and were converted to Jy/pixel using the above pixel and beam sizes within HIPE. The background sources outside the Helix and known sources across the Helix were subtracted using SExtractor and the images were sky subtracted within HIPE. It is possible that some contaminating hitherto unknown sources (mainly background galaxies) remain across the nebula. The resulting images are presented in Fig. 1

3. Dust Morphology

Only a bit of the outer halo and arc in the north is detected. Hence we will restrict the discussion in this paper to the main nebula. The region considered is indicated on the greyscale image in Fig. 1.

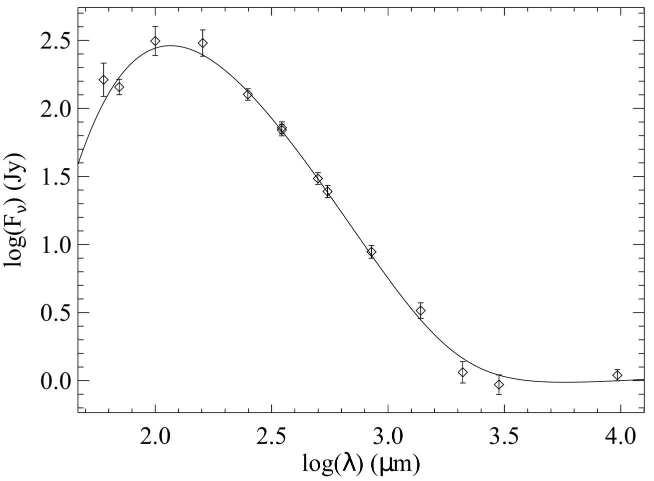

Fig. 2. The SED of NGC 7293 including IRAS, *Herschel* PACS and SPIRE, and Planck datapoints and a modified blackbody as in Eq. 2 with β=0.99. and T_{dust}=30.8 K

? noted that the structure of the Helix projects as if it were a thick walled "barrel" composed of red- and blue-shifted halves in a bipolar geometry. The barrel axis of the Helix is tilted about 10° east and 6° south relative to the line of sight (**?**). The barrel rims are widely separated in space, but the projected barrel shape, creates a false impression of the inner and outer circular structures. The apparent so-called “inner ring” is actually spatially distant velocity components projected together to create the illusion of a circle. Similarly, the apparent so-called “outer ring” is an artifact of the bulging central wall of the barrel, pushed outward to the east and west.

In the SPIRE maps we look at the cold dust without emission from atomic ions. The best compromise of resolution and signal is provided by the SPIRE 250 μm MD map (Fig. 1). The barrel wall is very fragmented and consists of emission clumps on size scales down to the resolution of the map. In the N we look more at the outer edge of the barrel, while in the S we look more down the barrel towards the central star. The dust emission is fainter when we look inside the barrel, and brighter when we look at the outside of the barrel wall. There appears to be less dust in the NW, which is in the direction of the receding plume. These plumes in the NW and SE appear as a radial flow-like structure in the WISE and GALEX images (see greyscale image in Fig. 1). They may be caused by a bipolar outflow with somewhat higher velocity puncturing wholes in the barrel walls (**?**). The plume in the SE is broader but less obvious, because we are looking inside, down the barrel towards the central star. The inner and outer side of the barrel appear well separated except in the SSW and in the N. Here the dust emission is bright, and also two extensions in the NNW and another one in the SSE. These are the edges of the barrel lobes.

Adopting the thick walled barrel bipolar morphology as proposed by **??** we notice that the dust emission comes mainly from the barrel wall. The dust emission is strongest where we look from the outside at the barrel, and is weaker when we look inside the barrel towards the central star.

4. Spectral Energy Distribution

In Fig. 2 we present the Spectral Energy Distribution (SED) of the Helix nebula. We retrieved the Planck images from the

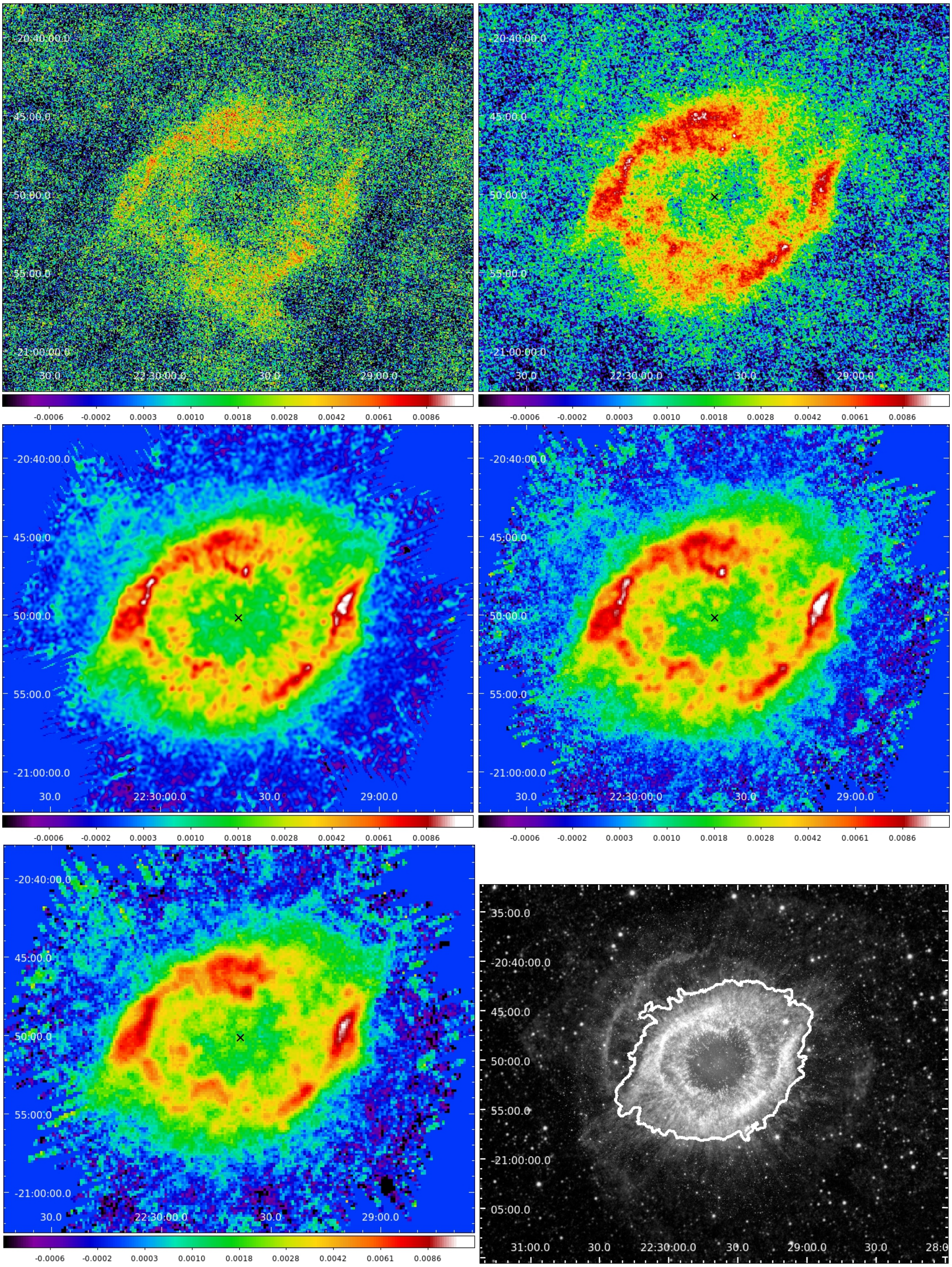

Fig. 1. *Herschel* images of NGC 7293. Top row left to right show the PACS 70 and PACS 160 μm images, the second row the SPIRE 250 and SPIRE 350 μm images, and the bottom row the SPIRE 500 μm and a NASA/JPL-Caltech composite image. The colorbar under the *Herschel* images shows the flux density in Jy/pixel. The grey scale image is the NASA/JPL-Caltech composite image (pia15817.html) including infrared data from Spitzer wavelengths 3.6 to 4.5 μm and 8 to 24 μm, WISE data at 3.4 to 4.5 and 12 to 22 μm, and ultraviolet data from GALEX at 0.15 to 2.3 μm. The region observed by *Herschel* and considered in this paper is indicated by the white contour in this last image.

Table 1. The photometric imaging observation log of the Helix nebula with *Herschel*

OD	RA (J2000.0)	DEC(J2000.0)	AOT	Duration	Start Date & Time	Obsid
350	22h29m38.55s	-20d50m13.60s	SpirePacsParallel	4326s	2010-Apr-28T22:30:39	1342195681
350	22h29m38.55s	-20d50m13.60s	SpirePacsParallel	4116s	2010-Apr-28T23:43:58	1342195682
1304	22h29m35.24s	-20d50m40.51s	SpirePhotoLargeScan	2047s	2012-Dec-08T10:54:32	1342256744

Table 2. The far infrared continuum fluxes measured by various satellite missions and the CBI. The second column gives the quoted flux, the third column the conversion factors from point source calibration to extended source calibration for the SPIRE data, the fourth column the color correction factor, and the fifth column the actual flux with all corrections applied.

Instrument	λ μm	K_{4E}/ K_{4P}	K_{color}	flux Jy	error Jy	fit Jy
IRAS	60	1.0000	0.9457	162.3	52.9	92.6
IRAS	100	1.0000	0.9650	312.8	87.0	271.9
PACS	70	1.0000	0.9961	143.6	19.9	151.8
PACS	160	1.0000	0.9996	302.0	75.3	251.2
SPIRE	250	0.9828	0.9978	126.7	12.9	135.6
SPIRE	350	0.9843	0.9991	69.4	7.2	69.6
SPIRE	500	0.9710	0.9788	30.6	3.2	30.8
Planck	350	1.0000	1.0190	72.0	7.6	69.6
Planck	550	1.0000	1.0881	24.5	2.7	24.5
Planck	849	1.0000	1.0983	8.83	1.00	8.42
Planck	1382	1.0000	1.1016	3.27	0.46	2.81
Planck	2096	1.0000	1.0077	1.15	0.23	1.46
Planck	2998	1.0000	1.0695	0.93	0.17	1.10
CBI	9671	1.0000	1.0000	1.10	0.11	1.00

Planck database and converted the units to Jy/pixel (see also **?**). We determined the integrated flux down to 0.008 Jy/pixel in the Planck 350 μm image, which corresponds to about 3 σ. We used this contour to measure the flux values at all other Planck wavelengths at 350, 550, 849, 1382, 2096, 2998 μm, but also used the same region within this same contour to measure the flux values in the SPIRE 250, 350, 500 μm parallel mode images, and the PACS 70 and 160 μm parallel mode images convolved to the SPIRE 250 μm beam and rebinned to its pixel size with flux conservation. We also retrieved the IRAS 60 and 100 μm images, but used a different contour as the IRAS beams were too large and too much flux would have been missed. We added a point at 31 GHz (9671 μm) from **?** obtained with the CBI interferometer in Chile (**?**) to constrain the free-free emission. Photometric color corrections were applied to all flux densities. This correction is needed to convert monochromatic flux densities that refer to a constant energy spectrum, to the true object SED flux densities at the photometric reference wavelengths of each instrument. The data are summarized in Table 2. Since the source is extended, the appropriate correction for extended source calibration were applied to the SPIRE fluxes:

$$F_\nu[\text{actual}] = \frac{K_{4\text{E}}}{K_{4\text{P}}} \frac{F_\nu[\text{quoted}]}{K_{\text{color}}} \tag{1}$$

The correction factors are given in Table 2. We note that the definition of K_{color} is the inverse of the definition used in the SPIRE Observer's Manual, but agrees with the definition used by the other instrument teams.

The Planck fluxes are a bit lower, but up to 2096 μm (143 GHz) within the error bars of the flux values mentioned in **?**. This is because the contours have been optimized for the SPIRE images where the beam and pixel sizes are smaller and the region considered more adjusted to the nebula. The percentage differences in flux values at longer wavelengths are larger because the flux values are low and the background more significant, compared to the shorter wavelengths (higher frequencies).

The thermal radiation emitted from a population of dust particles depends on their temperature distribution and opacity. Assuming that the opacity index varies with the frequency as a power law, i.e. $\kappa_\nu = \kappa_0(\nu/\nu_0)^\beta$, and that the dust grains dominating the flux in the IR and submm part of the SED all have the same temperature T_{dust} and the dust emission is optically thin, then the flux density spectral distribution can be approximated with a modified blackbody function of that temperature, plus a contribution by the free-free emission given by:

$$F_\nu = C\nu^\beta B_\nu(T_{\text{dust}}) + S_{1GHz} * (\nu/1\ GHz)^{-0.1} \tag{2}$$

where ν is the frequency and B_ν the Planck function of the dust temperature T_{dust}. The power law exponent, β, of the opacity law, basically depends on material properties and the size distribution of the dust grains. An exponent $\beta \approx 0$ would point to grains radiating almost as blackbodies (**?**).

We made χ^2-minimisation fits to available photometry data (weighted with the accuracy of the flux density measurement) and a contribution for the free-free emission. We obtained a dust emissivity index β=0.99 ± 0.09 and dust temperature T_{dust}=30.8 K ±1.4 K. Both measured and fitted values are presented in Table 2 and the best fit model in Fig. 2. A dust emissivity of slightly less than 1.0 was also found in both C-rich and O-rich (post-)AGB stars. This indicates that the dust has a layered amorphous structure (**?**). Based on laboratory measurements, a β value of 1 is more typical for amorphous carbon grains than for silicate grains (**??**). The Planck collaboration found a temperature of 34 K (no error bar given) and the amorphous carbon grain composition based on modelling the SED with DUSTY (**?**). DUSTY assumes spherical symmetry for the dusty envelope and the authors used a r^{-2} density distribution as first approximation to the nebular parameters.

The composition of the progenitor star in the Helix is still a subject of debate. Measurements by **?** of atomic emission lines in the nebula at one position in the north-eastern rim indicate that C/O is 0.87 ±0.12 suggesting that hot-bottom burning on the late AGB converted much of the ^{12}C into ^{14}N. However, the presence of CN, HCN, HNC, c-C_3H_2, and C_2H measured at one position in the eastern part of the Helix indicates a C-rich environment (**?**). In view of the carbon richness of the Helix molecular envelope, the absence of the familiar PAH emission features in the ISOCAM CVF (**?**) and IRS spectra (**?**) spectra is surprising. The absence of PAH emission bands in the mid-infrared spectra implies that no small dust particles are present in the envelope of this evolved PN (**?**) as they may have been destroyed during PN evolution, or it may be a sensitivity effect (**?**). The fact that dust grains are larger than typical grains in the ISM has been seen in other PNe such as NGC 650 (**?**) and NGC 6445 (**?**) for example. Several explanations were proposed in **?**, but the most plausible explanation could be that the large grains formed already during the AGB stage.

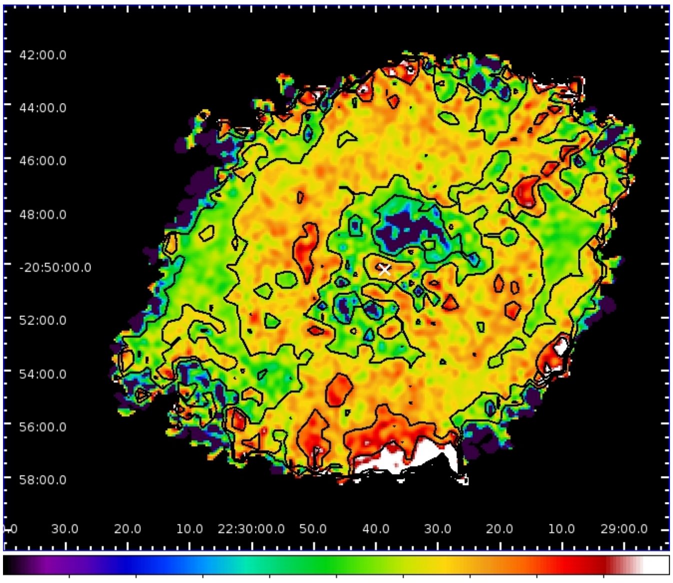

Fig. 3. Temperature map of NGC 7293 based on convolved PACS 70 μm and SPIRE 250 μm MD images. The temperature scale is shown below and the contours are at 22, 31, and 35 K.

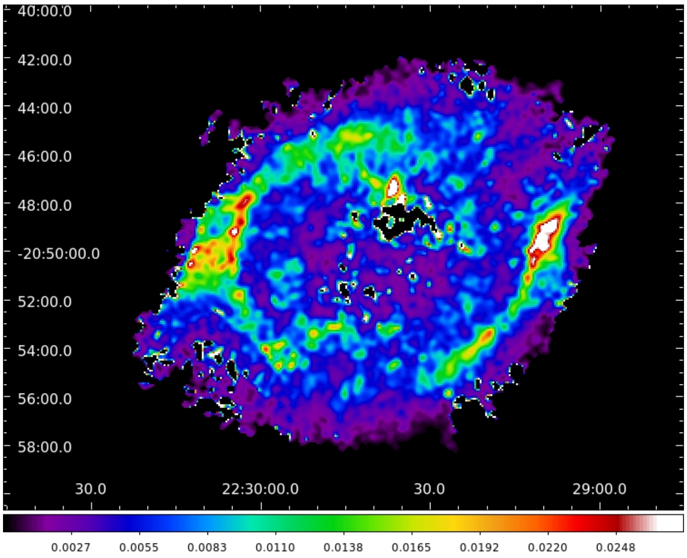

Fig. 4. Dust mass column density map of NGC 7293 based on SPIRE 250 μm MD image and the temperature map. The mass density scale is shown below in $M_\odot/pc^2$.

5. Temperature map

In order to make the temperature map, the PACS 70 μm sky subtracted image was convolved to the SPIRE 250 μm beam using the appropriate convolution kernels of **?** with flux conservation and rebinned to the pixel size of 4.″5. We computed the ratio of this convolved PACS 70 μm image to the SPIRE 250 μm MD image. In order to convert the flux ratio image to temperature map we computed the ratio of modified black body flux values at different temperatures using β=1.0 folded with the PACS and SPIRE filter transmission curves available in HIPE (v.8.0.1387), using the procedure outlined in the SPIRE Observer's Manual. We interpolated the flux ratio as a function of temperature for each pixel in the ratio image to obtain the temperature map (Fig.3). The central star position is marked with a white cross. We clipped the temperature image to the 1σ contour of the sky subtracted SPIRE 250 μm image.

The dust temperature is generally between about 22 K and 42 K. The dust is warmest in low density regions irradiated directly by the central star, and is cooler in dense regions and regions further away from the central star and/or shielded from direct starlight. We notice a warmer ring-like structure. This ring-like structure encompasses the inner side of the barrel as defined by **?**. The temperature in the barrel wall is not at all uniform but reflects its clumpiness. The extensions in the SE and NW are cool, high opacity regions at the outside of the barrel further away from the central star and shielded from direct starlight. Towards the plumes in the NW there are clumps of higher temperature. The higher temperatures in the S are mainly due to the excess emission in the PACS 70 μm map. As we are looking down the inside of the barrel towards the central star, it may well be that the temperature is higher. At other wavelengths there are also indications of a higher temperature in this region. Because of the low signal-to-noise ratio in the 70 μm map and the lower emission in the SPIRE 250 μm map at the southern edge, we can't be very sure of exactly how warm this region would be. It is reasonable to assume that it is not much warmer than other regions in the center of the nebula, where the temperature is about 40 K.

6. Dust mass column density

We calculated the dust mass column density for each pixel based on the temperature and the SPIRE 250 μm MD image using the formula of **?** and **?** (Fig. 4). The dust mass density image is not uniform, but reflects the clumpiness of the Helix nebula. The densest regions are regions where we look at the edge of the barrel. Integrating values in the map and assuming a distance of 216 pc the total dust mass of the Helix is 3.5 10^{-3} $M_\odot$.

As in **?** we have assumed a bulk density of $\rho_{gr} = 3\ g\ cm^{-3}$. According to **?** paper this value would be more appropriate for silicate grains. Because, from their SED fitting with DUSTY it appears that amorphous carbon was most appropriate for the dust composition, they used a value of $\rho_{gr} = 2\ g\ cm^{-3}$. They also used a distance of 213 pc instead of 216 pc. When we use these values we find a total dust mass of 3.4 10^{-3} $M_\odot$, which is in agreement with their value of 3.6 10^{-3} $M_\odot$ from their DUSTY modelling.

When we compare the dust temperature map Fig. 3 with the mass column density Fig. 4 map we notice that the dust temperature is about 31 K where the mass density is highest, and above 38 K where the density is lower.

7. Properties of the central star disk

? detected a pointlike source coincident with the central star, and a plateau of diffuse emission at 24 μm image, but only a pointlike source of flux 224 ± 33 mJy at 70 μm, and no point-like or extended emission at 160 μm with Spitzer. We convolved the PACS images to the SPIRE 250 μm beam using a pixel size of 4.″5 (see Fig. 5) and also noticed the presence of the central source at 70 μm, with a flux of 239 ± 24 mJy (i.e. in good agreement with Su et al.), but not at longer wavelengths, and no diffuse emission at any wavelength. Combining the 24 and 70 μm flux and our upper limits would imply a temperature of at least 65 K for the debris disk, and a mass of around 2 10^{-7} $M_\odot$, whith a large degree of uncertainty due to the upper limits.

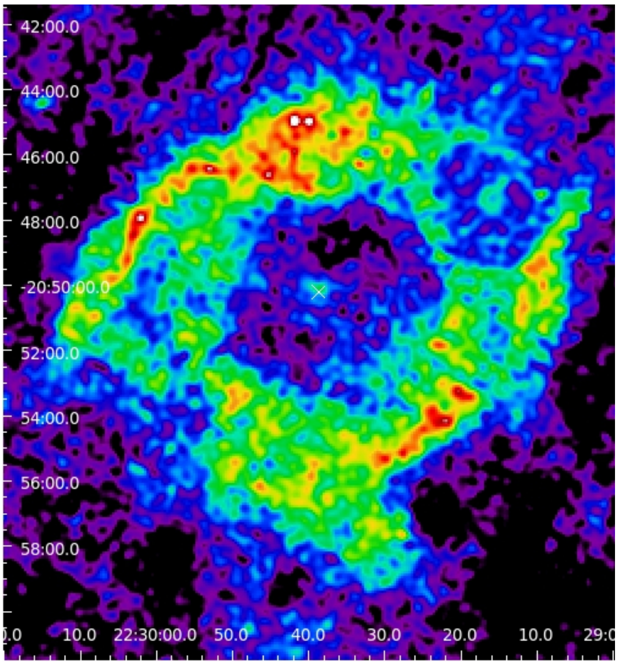

Fig. 5. PACS 70 image convolved to the SPIRE 250 μm beam with the central star disk indicated with a white cross.

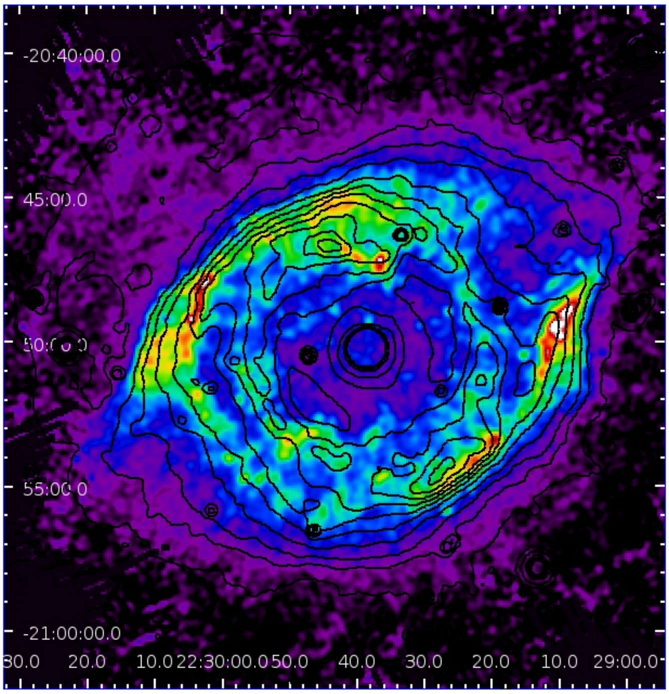

Fig. 6. SPIRE 250 μm MD image with the contours of GALEX NUV image convolved to SPIRE 250 μm beam overlaid.

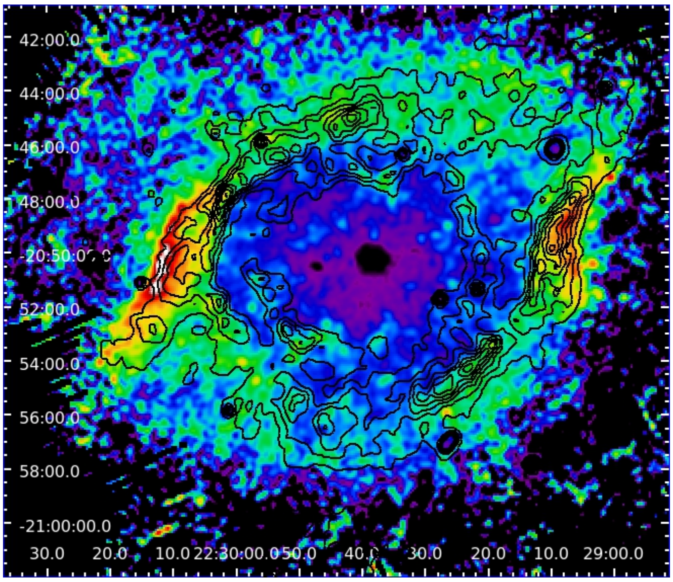

Fig. 7. The ratio of the SPIRE 250 μm image to the NUV GALEX image with the H_2 1−0 S(1) contours of **?** overplotted.

8. Comparison with images at other wavelengths

8.1. Comparison with GALEX images

In Fig. 6 we compare the NUV (175 - 280 nm) GALEX image (retrieved from the GALEX archive) convolved to the SPIRE 250 μm beam with the SPIRE 250 μm MD image. We notice that in the GALEX image the region inside the barrel is brighter than the outer barrel wall. In the SPIRE 250 μm image it is the other way round: the outside of the barrel is brighter than the inner wall. There is UV emission to the same spatial extent as the dust emission, but we see that the brightest dust emission is located just outside the bright emission in the NUV image. The UV emission is strongest at the edge of the inner cavity while the far infrared emission comes from the outer edge of the barrel.

In Fig. 7 we show the ratio of the dust image to the GALEX NUV image. As mentioned before this image emphasizes the fact that the dust emission is clumpy and the NUV emission is passing in between the clumps. The dust emission is strongest relative to the NUV emission in the extension in the SE. It is remarkable as the dust emission in the SPIRE 250 μm map nor the dust density seems particularly strong in that region. Here the dust appears to be shielded most from the UV emission. We are looking face on at the outer part of the barrel wall. This extension is moving towards us in the HCO$^+$ map of **?**. The extension in the NW has more complex kinematics and in part is moving away from us. It is the projection of the rim of the barrel lobe more towards the back of the Helix. It must be illuminated by the radiation passing through the holes. For the region in the south where there is relatively little dust emission compared to the NUV emission, we are looking down the barrel with blueshifted HCO$^+$ velocities in front ant red shifted velocities towards the back of the barrel. This is the region where there seems to be an excess in 70 μm emission (Fig. 1), a somewhat higher temperature (Fig. 3) and on average lower dust column density (Fig. 4).

In summary, the dust emission is strongest compared to the NUV emission where we look at the outside of the barrel of the Helix and the dust emission is most shielded from the UV radiation. The dust is clumpy and UV radiation must leak through.

8.2. Comparison with the H_2 image

We convolved the H_2 image of **?** with the SPIRE 250 μm PSF (**?**). The resulting comparison is shown in Fig. 8. The contours of this convolved H_2 image are overlaid on the SPIRE 250 μm image to the right. We see that the contours overlap: the H_2 emission comes from the same region as the dust emission. The peaks

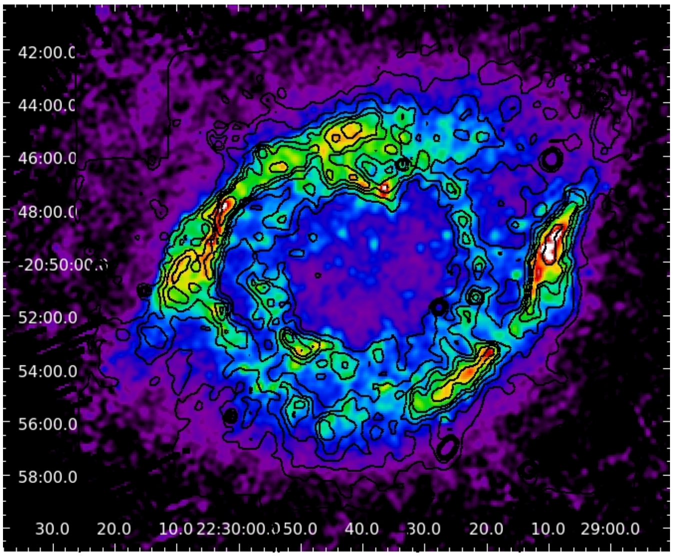

Fig. 8. The contours of the H_2 1−0 S(1) image convolved to the SPIRE 250 μm beam are overlaid on the SPIRE 250 μm image

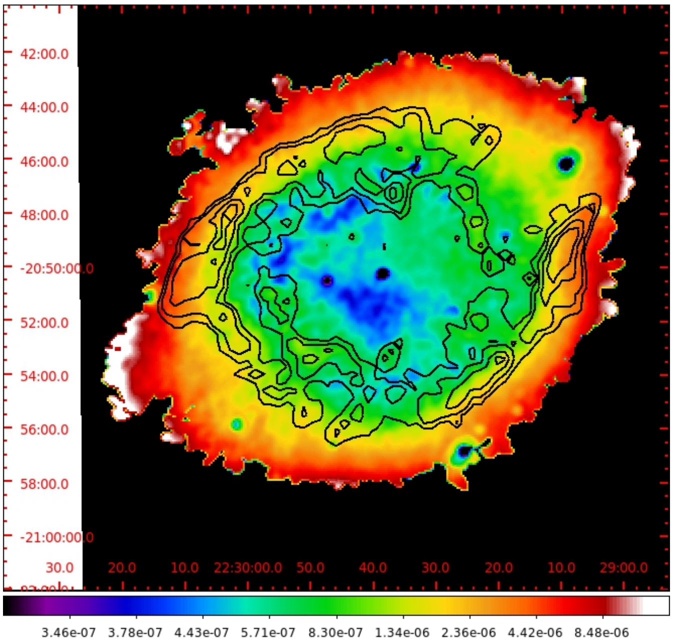

Fig. 9. The ratio of the H_2 to the Hβ image both convolved to the SPIRE 250 μm beam (displayed in log scale) with the dust SPIRE 250 μm contours overlayed.

of the H_2 emission and the dust emission agree, except in the south. The H_2 emission is relatively strong compared to the dust emission in the south and the peaks don't seem to coincide. This is the region where we look down the barrel towards the central star.

The gas kinetic temperature T_k was found to be about 20 to 40 K (**??**), which is similar to our determined dust temperature. The gas density of the H_2 emission is of the order of n(H_2)∼ (1-5) 10^5 cm^{-3}. At gas densities higher than $10^{4.5}$ cm^{-3} the dust and gas temperatures will be closely coupled (**?**). It is another indication that, as is the case in the Ring Nebula (**?**) and NGC 650 (**?**), in NGC 7293 H_2 and dust also co-exist in dense clumps, "knots", that are embedded in the ionized gas ((**?**)). This close correlation could be an indication of the formation of H_2 on dust grains.

Exactly when the knots formed during the evolution is still debated. These knots may be density enhancements formed during the AGB phase in the shell and survived the ionization of the nebula (**??**). Or they may have formed due to instabilities and fragmentation at the ionization front when the nebula got ionized (**??**). As knots are observed in older PNe having central stars well evolved on the cooling track, it has been suggested that they formed due to hydrodynamical instabilities when the nebular gas is going through recombination phase (**??**). The formation of H_2 most effectively takes place on the surface of dust grains, also at grain temperatures as found here for the Helix nebula (**??**). The high density in the knots makes it possible to shield the H_2 from the stellar radiation field. The high densities and low dust temperatures observed allow to re-form H_2 molecules on dust grains on a reasonable timescale (**?**). H_2 formation in the knots is expected to be substantial after the central star entered the cooling track and underwent a strong drop in luminosity, and may still be ongoing at this moment, depending on the density of the knots and the properties of the grains in the knots and assuming the knots formed quickly. Especially in the latter case we expect a tight correlation between the dust emission and the H_2 emission (**?**) as is observed now in the Helix nebula.

The possible effect of the UV emission on the H_2 is investigated in Fig. 7. H_2 contours are overlaid on the ratio of the SPIRE 250 μm image to the NUV Galex image. We see that the strong dust and H_2 emission originate just outside the peaks of NUV emission at the edges of the nebula and in the extensions. It is in these regions where the H_2 and dust emission coincides best. When we overplot the H_2 contours on the ratio image of the SPIRE 250 μm MD to NUV images, we notice that the H_2 emission is situated at the inner edge where this ratio is very high. This is in agreement with what was found by **?**: if the cometary knot is beyond the Helix ionization front, then there is no ionized region, the knot is completely neutral and there would be not enough radiation or temperature to excite significantly the upper vibrational levels of the molecule. The 1–0 S(1) intensity would be very low. In the south where there is relatively more NUV flux to dust emission the H_2 emission is relatively strong.

To compare the molecular with ionized component we obtained an Hβ image from **?** and **?**. We convolved the image to the SPIRE 250 μm PSF (**?**) with flux conservation and rebinned it to a pixel size of 4″.50. We took the ratio of the convolved H_2 image to this Hβ image. The resulting image is shown in Fig. 9. The density structure has virtually disappeared and we see the rapid decrease of the ionizing radiation field outwards beyond the inner ring. We see that the ionized region is mainly contained within the molecular and dust region. The dust and molecular emission is not particularly strong inside the barrel, because the influence of the stellar radiation field is significant.

9. Conclusion

We presented *Herschel* PACS and SPIRE images of the Helix nebula. The dust emission is clumpy and present in the barrel wall. We presented consistent photometry of the Helix without its halo and determined its spectral energy distribution. The emissivity index of $\beta = 0.99 \pm 0.09$, in combination with the carbon rich molecular chemistry of the nebula, indicates that the dust consists mainly of amorphous carbon. We determined an average dust temperature of 30.8 K ± 1.4. We detected the central star disk at 70 μm, confirming the result of **?**. At other wavelengths we only have upper limits, hence the dust temperature of the disk of 65 K is only an estimate. The dust mass column density map reflects the clumpiness of the dust. The dust mass of the main nebula of $\sim 3.5\ 10^{-3}\ \mathrm{M}_{\odot}$ at a distance of 216 pc. The temperature map shows a variation in dust temperature between $22-42$ K. This is similar to the kinetic temperature of the molecular gas and indicates that the dust and molecular gas co-exist in very dense clumps. We compared the SPIRE 250 μm image with images at other wavelengths to determine the extent and morphology of the dust, molecular, and ionized component in the nebula. The morphology of the different components can be understood adopting the thick walled barrel-like model tilted about 10° east relative to the line of sight from **?**. The radiation field decreases rapidly outwards in the barrel wall. The very good coincidence between the H_2 and the dust emission in the barrel wall suggests the formation of H_2 on dust grains.

Acknowledgements. Herschel is an ESA space observatory with science instruments provided by European-led Principal Investigator consortia and with important participation from NASA. PACS has been developed by a consortium of institutes led by MPE (Germany) and including UVIE (Austria); KU Leuven, CSL, IMEC (Belgium); CEA, LAM (France); MPIA (Germany); INAF-IFSI/OAA/OAP/OAT, LENS, SISSA (Italy); IAC (Spain). This development has been supported by the funding agencies BMVIT (Austria), ESA-PRODEX (Belgium), CEA/CNES (France), DLR (Germany), ASI/INAF (Italy), and CICYT/MCYT (Spain)." SPIRE has been developed by a consortium of institutes led by Cardiff University (UK) and including Univ. Lethbridge (Canada); NAOC (China); CEA, LAM (France); IFSI, Univ. Padua (Italy); IAC (Spain); Stockholm Observatory (Sweden); Imperial College London, RAL, UCL-MSSL, UKATC, Univ. Sussex (UK); and Caltech, JPL, NHSC, Univ. Colorado (USA). This development has been supported by national funding agencies: CSA (Canada); NAOC (China); CEA, CNES, CNRS (France); ASI (Italy); MCINN (Spain); SNSB (Sweden); STFC (UK); and NASA (USA) HCSS / HSpot / HIPE is a joint development (are joint developments) by the *Herschel* Science Ground Segment Consortium, consisting of ESA, the NASA *Herschel* Science Center, and the HIFI, PACS and SPIRE consortia. This research made use of tools provided by Astrometry.net. Some of the data presented in this paper were obtained from the Multimission Archive at the Space Telescope Science Institute (MAST). STScI is operated by the Association of Universities for Research in Astronomy, Inc., under NASA contract NAS5-26555. Support for MAST for non-HST data is provided by the NASA Office of Space Science via grant NNX09AF08G and by other grants and contracts. P.v.H. and the PACS ICC in Leuven wish to acknowledge support from the Belgian Science Policy office through the ESA PRODEX programme. ME, JRG and JC thank the Spanish MINECO for funding support from grants CSD2009-00038, AYA2009-07304 and AYA2012-32032.